RSC Advances

ROYAL SOCIETY OF CHEMISTRY

www.rsc.org/advances

RSC Advances

PAPER

A self-assembled Si/SWNT 3D-composite-nanonetwork as a high-performance lithium ion battery anode

Received 00th January 20xx,
Accepted 00th January 20xx

DOI: 10.1039/x0xx00000x

www.rsc.org/

Xiurong Guan[a], Lina Wang[a b], Jia Yu[b], Yuchao Li[b], Shimou Chen*[b] and Suojiang Zhang*[b]

In this work, we have prepared a 3D-composite-nanonetwork material consisting of single walled carbon nanotube (SWNT) network and Si nanosphere embedded elements, through an electrostatic induced self-assembly process and the following film transfer technique. Negatively charged acid-functionalized SWNTs and positively charged surface-modified Si nanospheres composed a highly dispersed system, which was key to the fabrication of self-assembled active material film. After transferring it to the Cu foil substrate by a novel film transfer technique, an integrated anode for lithium ion batteries (LIBs) was obtained without using of binders or conductive additives, and exhibited excellent electrochemical performance. The continuous 3D conductive network consisting of SWNTs provided a rapid electronic transport pathway, which was able to counteract the conductivity decline caused by the formation of solid electrolyte interface layer, thus ensuring a superior rate capability and cycling stability. This combined process of self-assembly and film transfer would provide a new idea for the design and preparation of LIB electrodes, especially which were restricted by low conductivity and large volume change during cycling.

Introduction

High efficient energy conversion and storage devices have became the core components in many emerging applications.[1-3] From electric vehicles to wearable electronics, lithium ion batteries (LIBs) have been considered as a dominant power source, due to their high energy density, long cycle life and environmental friendliness.[4-6] The electrode material dominates the electrochemical performance of LIBs to a great extent, but the common graphite anode only exhibits a limited capacity of 372 $mAhg^{-1}$ which hardly meet the increasing demand for performance.[7-9] Therefore, numerous efforts have been made to develop alternative anode materials with higher specific capacity and better stability. Among widely studied next-generation anodes, silicon has attracted special attention owing to its theoretical capacity as high as 4200 $mAhg^{-1}$ which is ten times higher than that of graphite, and an appropriate working voltage (<0.5V vs Li^+/Li).[10-14]

However, two major drawbacks restrict the practical application of Si as a LIB anode. On one hand, Si demonstrates a dramatic volume change (>300%) during the Li^+ intercalation-deintercalation process, resulting in pulverization of anodes.[15-19] First, the pulverization would cause an excessive formation of solid electrolyte interface (SEI) layer which leads to a high capacity loss during cycling.[20] Second, the pulverization would damage the mechanical adhesion and electrical contact between active materials and current collectors, thus a rapid capacity fading. On the other hand, low conductivity of Si hinders its performance at high rates, which was currently the focus of LIB development.[21,22] Aiming at these challenges, one strategy is to design Si nanostructures such as nanoparticles,[23,24] nanowires,[25,26] nanotubes[27] and nanospheres.[28] The nanostructures can provide a larger electrode/electrolyte interface, a reduced diffusion path for both Li^+ ions and electrons and larger free volume to buffer the expansion, improving the rate and cycling performance.[29] Another strategy is combining Si with high conductive and low expansive carbon material, such as carbon nanotubes (CNTs),[30,31] graphene[32,33] and porous carbon,[34] to promote electron transfer and accommodate volume change. However, the effect of single-strategy is usually very limited, thus multiple strategies should be combined for efficiently enhancing the performance. Based on above discussion, various approaches have been successfully carried out to fabricate Si/C composites. For example, Bradford et al. fabricated an aligned CNT-Si sheet structure with the chemical vapor deposition (CVD) method, delivering an excellent specific capacity of 1494 $mAhg^{-1}$ after 45 cycles.[17] Tu et al. synthesized a Si/porous reduced grapheme oxide (rGO) composite by steam etching of Si/rGO aerogel, leading to good cycling performance with 1004 $mAhg^{-1}$ after 100 cycles.[35]

In our work, we have fabricated a Si/SWNT 3D-composite-nanonetwork material, basing on an aqueous-based electrostatic induced self-assembly process and the following

[a] School of Environmental and Chemical Engineering, Shenyang ligong University, Liaoning 110159, PR China. E-mail: guan7551@sina.com
[b] Beijing Key Laboratory of Ionic Liquids Clean Process, Key Laboratory of Green Process and Engineering, State Key Laboratory of Multiphase Complex Systems, Institute of Process Engineering, Chinese Academy of Sciences, Beijing 100190, PR China. E-mail: chenshimou@ipe.ac.cn
† Footnotes relating to the title and/or authors should appear here.
Electronic Supplementary Information (ESI) available: XPS spectra, TEM-EDS analysis, SEM images, SEM-EDS Mapping analysis and TGA curves. See DOI: 10.1039/x0xx00000x

novel technique of film transfer. The highly dispersed system consisting of negatively charged acid-functionalized SWNTs and positively charged Si nanospheres modified by poly(diallyldimethylammonium chloride) (PDDA), was the key to the self-assembly.[36,37] And after transferring the composite active material film to the Cu foil substrate using a film transfer technique, an integrated LIB anode was obtained. For this 3D-composite-nanonetwork, Si nanospheres were well dispersed and connected to the SWNT network, bringing a series of advantages on Li-storage performance: 1) The SWNTs provided a high conductive 3D network framework, which was able to provide a rapid electron transport path under the formation of SEI layer. 2) The embedment of Si nanospheres into the network consisting of high strength SWNTs would alleviate the volume change of Si during charge-discharge process to some extent, alleviating the pulverization. Moreover, the embedding effect prevented the peeling of Si nanospheres from the current collectors. 3) Compared with traditional LIB anodes, the integrated anodes exhibited a higher loading density of active materials because of the absence of binders and conductive additives, with a superior mechanic adhesion and electrochemical contact.[38] This Si/SWNT 3D-composite-nanonetwork anode exhibited an excellent electrochemical performance, being able to maintain a high capacity up to 941 $mAhg^{-1}$ after 50 cycles, at a current density of 400 mAg^{-1}. Moreover, this combined process of electrostatic induced self-assembly and film transfer would provide a new idea for the design and preparation of next generation LIB electrode materials, especially which were restricted by low conductivity and large volume change during cycling.

Experimental

Preparation of acid-functionalized SWNTs

Original SWNTs were purchased from XFnano, with an average diameter of 10~20 nm and an average length of 5~30 μm. The SWNTs were refluxed in concentrated HNO_3/H_2SO_4 (1/3 V/V) for 3h to prepare carboxylic acid-functionalized SWNTs.[39] After refluxing, the mixture was centrifuged and re-dispersed for several times in turn to remove the excess mixed acid. Finally, the mixture was filtered using a nylon membrane and then dried at 80 ℃ for 12 h.

Preparation of Si-PDDA nanospheres

Si nanospheres were purchased from Alfa Asar, with an average particle size of 40~50 nm and a purity of more than 98%. PDDA was purchased from Aladdin. 150 mg of Si nanospheres were added into 100 ml of deionized water, followed by addition of 0.5 ml of 35 wt% PDDA aqueous solution. The mixture was treated with ultrasonic for 30 min, and subsequently stirred for 2 h to obtain a homogeneous system, in which the PDDA-modified Si (or Si-PDDA) nanospheres were dispersed. And then it was centrifuged and re-dispersed for three times in turn, to remove the excess PDDA. Finally, the mixture was centrifuged at 4000 r/min for 15 min, and the supernatant liquid was reserved.

Preparation of Si/SWNT 3D-composite-nanonetwork anodes

First, 0.06 g of as-prepared acid-functionalized SWNTs was added into 600 ml of deionized water, then, the mixture was treated with ultrasonic for 2 h to obtain a dispersive solution. And this solution was centrifuged at 10000 r/min for 30 min, to obtain the supernatant liquid. Above mentioned supernatant of Si-PDDA nanospheres was added into the SWNT supernatant drop wise, with vigorous stirring. And after 30 min of ultrasonic treatment, a homogeneous dispersed system was obtained. Subsequently it was filtered through a mixed cellulose ester (MCE) filter membrane to achieve a Si/SWNT film. After dropping a few drops of ethanol on this film, the filter membrane was transferred onto the Cu foil. With the evaporation of ethanol, the Si/SWNT film was closely attached to the Cu foil substrate, followed by being immersed into acetone to dissolve the MCE filter membrane.[40] Therefore, finally this Si/SWNT composite film was successfully transferred from the membrane to the Cu foil, and a binder-free LIB integrated anode was obtained.

Characterization

The morphology and structure of the samples were characterized by scanning electron microscopy (SEM, JEOL JSM-7001F), transmission electron microscopy (TEM, JEOL JEM-2100). The composition was tested using an X-ray diffractometer (XRD, Rigaku, Smartlab) with a Cu-$K_{\alpha 1}$ radiation source (9 kW, λ=0.15406 nm) and X-ray photoelectron spectroscopy (XPS, PHI5700). The thermo gravimetric analysis was performed between room temperature and 800 ℃, with air atmosphere and a heating rate of 10 ℃/min (STA7200RV, Hitachi High-Tech). The Raman spectra were recorded using an 514 nm Ar-ion laser (LabRAM HR800, Horiba Jobin-Yvon). The energy dispersive spectrometry (EDS) analysis was carried out by Oxford X-Max^N with SEM and TEM.

Electrochemical measurements

Electrochemical measurements were carried out using a coin cell (LIR 2025). The as-prepared materials were directly used as the working electrode without any ancillary materials. The lithium foil was used as the counter and reference electrode, and the electrolyte was 1 M LiPF6 in EC/DEC/DMC (1:1:1, weight). Coin cells were assembled in an Ar-filled glove box. The galvanostatic charge-discharge tests were measured using a LAND battery testing system at 25 ℃, at a voltage range of 0.01-2.8 V. Electrochemical impedance spectroscopy (EIS) measurements tests were carried out on a ACM Gill-AC-4 electrochemical station.

Results and discussion

The preparation procedure of the Si/SWNT 3D-composite-nanonetwork integrated anode was exhibited, as shown in Scheme 1. First, the pretreatment process on SWNTs and Si

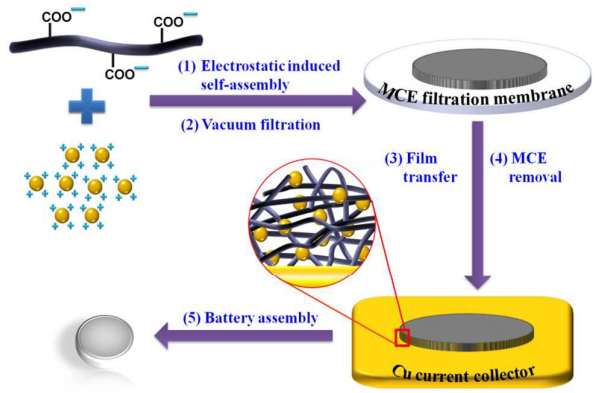

Scheme 1 the preparation procedure of the Si/SWNT 3D-composite-nanonetwork integrated anode for LIBs

nanospheres was the key to the successful fabrication of network framework. On one hand, during the backflow process carboxyl groups were generated on the SWNT surface, which made the SWNTs exhibit negative charges in aqueous media.[41] On the other hand, original Si nanospheres tended to exhibit negative charges in aqueous media because of the existence of SiO_2 on the surface.[42] When modified by PDDA, their surface charges became positive. The existence of PDDA on Si nanosphere surface was proved by XPS analysis (Figure S1, ESI) and TEM-EDS analysis (Figure S2). Subsequently, the aqueous solutions of Si-PDDA nanospheres and acid-functionalized SWNTs were mixed to obtain a uniform Si/SWNT dispersed systems. And then the Si/SWNT aqueous solution was filtered through a MCE filter membrane. At this stage, the 3D-composite-nanonetwork was fabricated, owing to the electrostatic induced self-assembly process in the highly dispersed system consisting of negatively charged SWNTs and positively charged Si nanospheres. Without the pretreatment process that changed surface charges orientationally, the network framework would hardly be constructed because of the aggregation effect. Subsequently, the obtained sample-loaded MCE membrane was transferred to a Cu foil. After dissolving the MCE membrane, a Si/SWNT composite film fabricated on the Cu foil substrate was successfully prepared, obtaining an integrated LIB anode. The fabrication method of this anode was facile, without using of binders or conductive additives.

The morphology and structure of the as-synthesized Si/SWNT 3D-composite-nanonetwork material was characterized by SEM and TEM (Figure 1). Si nanospheres with an average diameter of 40~50 nm were uniformly dispersed among the SWNTs with an average diameter of about 20 nm (Figure 1a). The SWNTs formed a continuous 3D carbon-based network framework, which would provide a fast electronic transport pathway for LIB anodes under the existence of the SEI layer. The high-magnification SEM (HRSEM) image clearly indicated that the Si nanospheres were embedded into the interspace of the SWNT network (Figure 1b). Accompanied with the strong mechanical strength of SWNTs, this embedding effect was able to alleviate the originally huge volume change of Si nanospheres during Li^+ intercalation-deintercalation process to some extent, and efficiently stabilize the active materials by preventing their peeling from the current collectors. As a contrast, we have also prepared similar Si/SWNT composite materials with the same experimental system and conditions, except for the absence of PDDA-modifying process on Si nanospheres. As shown in Figure S3, in this case, the Si nanospheres tended to aggregate into larger cluster instead of disperse. However, with PDDA-modifying process Si nanospheres were able to disperse uniformly, mainly because of the electrostatic attraction between positively charged Si-PDDA nanospheres and negatively charged acid-functionalized SWNTs, and the electrostatic repulsion among Si-PDDA nanospheres. In addition, functional groups on the Si-PDDA surface also provided steric hindering among nanospheres[22]. As shown in Figure 1c, the TEM image further confirmed the 3D-composite-nanonetwork structure. In high-magnification TEM (HRTEM) image, the combination between the SWNT and Si nanospheres was observed clearly (Figure 1d). In addition, the inset showed the highly crystalline nature of the Si nanosphere and a preferential (111) orientation

This composite material was further characterized by the SEM-EDS mapping, showing the presence of Si and C elements clearly, which corresponded to the Si nanospheres and SWNTs, respectively (Figure S4). The Raman spectrum of Si/SWNT was exhibited in Figure 2a, together with the spectrums for individual Si nanospheres and SWNTs as a contrast. For the Si/SWNT, the peak centered at 516 cm^{-1} was related to the Raman phonon vibration of crystalline Si. Meanwhile, the disorder band (D-band) at 1350 cm^{-1} and the strong graphitic

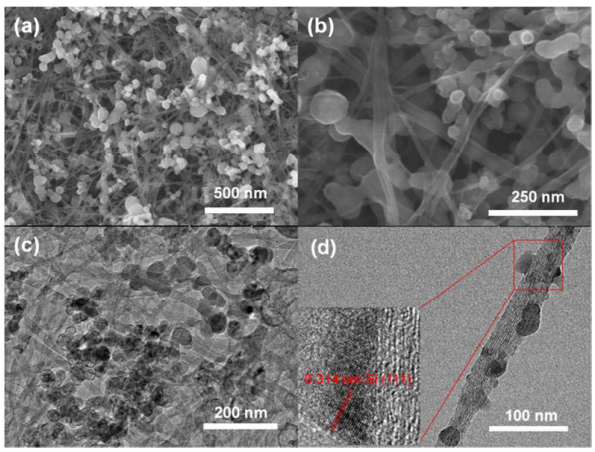

Figure 1 (a) SEM, (b) HRSEM and (c) TEM image of the Si/SWNT 3D-composite-nanonetwork material, Si nanospheres were uniformly dispersed among the SWNT network. (d) HRTEM image, Si nanospheres were combined with the SWNT, the inset showed crystalline Si and a preferential (111) orientation.

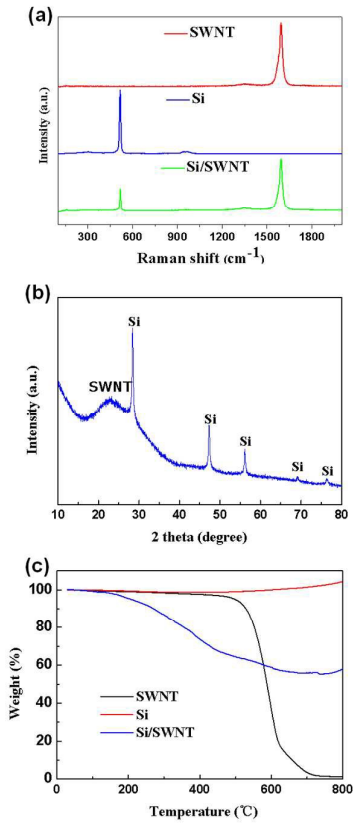

Figure 2 (a) Raman spectrum of the Si/SWNT, SWNT and Si. (b) XRD pattern of SWNT. (c) Thermal gravimetric analysis curves of the Si/SWNT, SWNT and Si.

band (G-band) at 1592 cm^{-1} were related to the SWNTs. All the peaks matched well with the individual SWNTs or Si nanospheres samples.[43] The crystalline structures of Si nanoparticles as well as SWNTs were not affected by the electrode fabrication procedure. Figure 2b showed the XRD pattern of this Si/SWNT composite material, which matched well with characteristic peaks of the SWNT and the Si.[19] In addition, to investigate the composition, TGA curves of Si/SWNT, Si nanospheres and SWNTs were measured under air atmosphere, from room temperature to 800 ℃ (Figure 2c). For SWNT sample, from the initial weight loss at about 400 ℃, they would be completely burned away at 800 ℃ (99% loss in weight). And for Si sample, the slight mass enhancement (4%) beyond 800 ℃ was owed to the oxidation of Si.[37] It exhibited that the weight percentage of Si in this composites was 54%, while the weight loss prior to 400 ℃ was attributed to the remove of PDDA.

The electrochemical performance of the Si/SWNT 3D-composite-nanonetwork material as a LIB anode was tested through a LIR 2025 coin cell. Above mentioned Si/SWNT sample which exhibited a 54 wt% Si component was named Si/SWNT-54 wt%. And similarly Si/SWNT-36 wt% and Si/SWNT-28 wt% were prepared, by adding various amount of Si supernatant liquid in the mixing step. Figure 3a displayed the charge and discharge curves of the Si/SWNT-54 wt% anode for the first three cycles, at a current density of 400 mAg^{-1} and a voltage window of 0.01~2.8 v VS Li^+/Li. The specific capacity was calculated against the total mass of the Si/SWNT composite. The initial discharge capacity was 1871 $mAhg^{-1}$ with a reversible charge capacity of 1321 $mAhg^{-1}$, showing an initial coulombic efficiency of 71%, because of the formation of the SEI layer.[8, 44] For comparison, the charge and discharge curves of the pure SWNT was also investigated at the same conditions

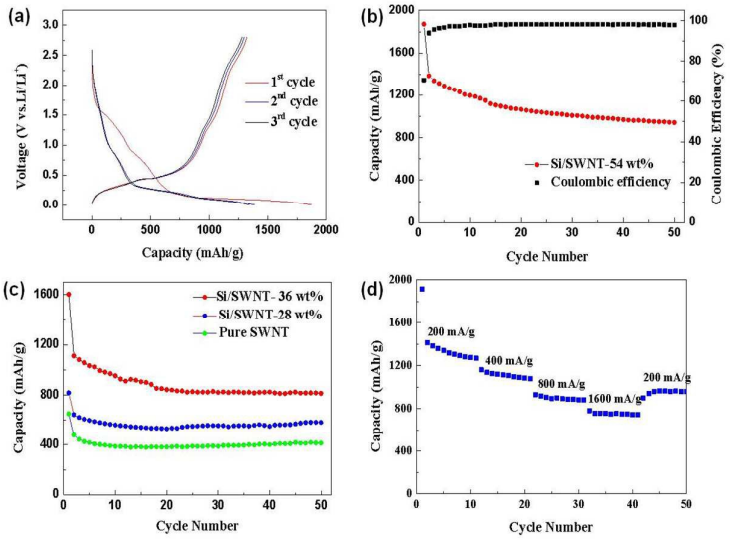

Figure 3 (a) First three charge/discharge profiles of the Si/SWNT-54 wt% at a current density of 400 mAg^{-1}. (b) Cycling performance and coulombic efficiency of the Si/SWNT-54 wt% at a current density of 400 mAg^{-1}. (c) Cycling performance of the Si/SWNT-36 wt%, Si/SWNT-28 wt% and pure SWNT at a current density of 400 mAg^{-1}. (d) Rate performance of the Si/SWNT-54 wt% at different current densities.

(Figure S5). The initial discharge capacity of the pure SWNT was 652 $mAhg^{-1}$, which proved that the addition of Si enhanced the specific capacity greatly. Figure 3b exhibited the discharge capacity vs cycle number curve and corresponding coulombic efficiency of Si/SWNT-54% anode. An good cyclic stability was observed without obvious capacity fading after 20 cycles. Its discharge capacity was maintained at 941 $mAhg^{-1}$ after 50 cycles at a current density of 400 mAg^{-1}, and the coulombic efficiency was stabilized at more than 98 % after 15 cycles. A continuous formation of the SEI layer usually caused a decrease of coulombic efficiency, which meant a higher irreversible capacity.[19] Therefore, it was indicated that our products formed a stable SEI layer, with a stable reversible capacity.

To investigate the effect of Si weight percentage on electrochemical performance of the Si/SWNT composite anode, the cycling performance of Si/SWNT-36 wt%, Si/SWNT-28 wt% and pure SWNT were investigated at the same condition as that of Si/SWNT-54wt% (Figure 3c). The thermal gravimetric curves of the Si/SWNT-36 wt% and Si/SWNT-28 wt% were shown in Figure S6. After 50 cycles, these three anodes exhibited discharge capacities of 814, 583 and 414 $mAhg^{-1}$, respectively, which were much lower than that of Si/SWNT-54 wt%. Obviously, the Si content was the key to the electrochemical performance of the composite anode. Moreover, rate capability of the Si/SWNT-54 wt% was shown in Figure 3d, with various current densities of 200, 400, 800 and 1600 mAg^{-1} and a voltage range of 0.01~2.8 v. Only a slight reduction of capacity was observed with the rate increasing. It was able to maintain a high specific capacity of more than 740 $mAhg^{-1}$ at a high current density of 1600 mAg^{-1}. When the current density recovered to 200 mAg^{-1}, it demonstrated a retention capacity of 950 $mAhg^{-1}$, demonstrating a good rate capability.

Figure 4a showed the Impedance spectra of the Si/SWNT-54 wt% anode before cycling and after 50 cycles. The depressed semicircle in the high-medium frequency represented the charge transfer impedance and the inclined line in the low frequency region was attributed to the lithium diffusion impedance.[21] It was obvious that the charge transfer impedance after 50 cycles was smaller than that before cycling.

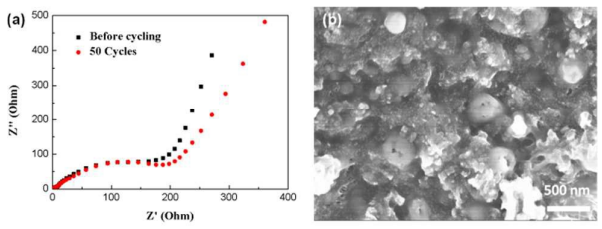

Fig. 4 (a) Impedance spectra of the Si/SWNT-54 wt% anode before cycling and after 50 cycles. (b) Morphology of the Si/SWNT-54 wt% anode after 50 cycles.

The excellent conductivity of Si/SWNT composite anode could be owed to the 3D SWNT conductive network which was able to counteract the conductivity decline caused by the formation of SEI layer. In addition, to investigate the structural stability during repeated cycling, the morphology of Si/SWNT-54 wt% anode after 50 fully lithiated cycles were observed. It still exhibited a stable skeleton of SWNT networks and uniformly dispersed Si nanospheres, showing a good cycling stability of this composite anode (Figure 4b). To illustrate the long-term adhesion between the active materials and the current collector, cross-section SEM images after 50 cycles was displayed in Figure S7 (ESI). There was no significant void between active materials and collector and they are well connected. It proved that there is strong long-term adhesion between active materials and current collector, which should be due to the strong interfacial van de Waals force between SWNT network and Cu collector.

In a word, the Si/SWNT 3D-composite-nanonetwork anode exhibited excellent cycling stability and rate capacity as a LIB anode, which was mainly owed to its unique structural features. First, SWNTs formed a continuous 3D carbon-based conductive network, which provided a fast electronic transport path to counteract the conductivity decline caused by the SEI layer, being favorable for a considerable rate performance. Second, this embedding of Si nanospheres into the network consisting of high mechanical strength SWNTs was able to buffer their dramatic volume change during Li^+ intercalation-deintercalation processes to some extent, alleviating the pulverization of the Si nanospheres and thus an improved cycling stability. Third, the embedding effect also stabilized the Si nanospheres by prevented their peeling from the current collectors, leading to a better cycling stability. Forth, owed to the film transfer process, this integrated anode had a stable mechanical adhesion and an excellent electrochemical contact between active materials and current collectors without using of binders or conductive additives, effectively enhancing the energy density and improving electrochemical performance.

Conclusions

In conclusion, herein we have successfully prepared a 3D-composite-nanonetwork architecture consisting of Si nanospheres and SWNTs. An integrated LIB anode without binders or conductive additives was obtained, after a film transfer process towards the Cu foil substrate. The key of the successful preparation was the electrostatic induced self-assembly process in a highly dispersed system, which was consisted of negatively charged acid-functionalized SWNTs and positively charged Si-PDDA nanospheres. For this Si/SWNT composite anode, a highly conductive SWNT network provided a rapid electron transport path, while the embedding of Si nanospheres alleviated their volume change during cycles and prevented their peeling from current collectors. Owing to its unique microstructure, the Si/SWNT composite anode exhibited an excellent electrochemical performance. It was able to maintain a discharge capacity as high as 941 $mAhg^{-1}$ after 50 cycles at a current density of 400 mAg^{-1}, with an

excellent rate capability, while the weight percent of Si was the key to the anode performance. The whole preparation procedure was facile and controllable, and it can be extended to other LIB electrode materials whose application was restricted by low conductivity and dramatic volume expansion.

Acknowledgements

This work was supported by National Key Basic Research Program of China (2015CB251401) and National Natural Science Foundation of China (No. 21276257, 21210006) and Beijing Natural Science Foundation (2132054) and "Strategic Priority Research Program" of the Chinese Academy of Science (Grant No. XDA09010103).

References

1 M. R. Zamfir, H. T. Nguyen, E. Moyen, Y. H. Lee and D. Pribat, *J Mater Chem A*, 2013, **1**, 9566-9586.
2 Y. F. Deng, Z. N. Li, Z. C. Shi, H. Xu, F. Peng and G. H. Chen, *Rsc Adv*, 2012, **2**, 4645-4647.
3 Y. Zhang, Y. Z. Jiang, Y. D. Li, B. B. Li, Z. H. Li and C. M. Niu, *J Power Sources*, 2015, **281**, 425-431.
4 B. Dunn, H. Kamath and J. M. Tarascon, *Science*, 2011, **334**, 928-935.
5 S. Y. Zheng, Y. Chen, Y. H. Xu, F. Yi, Y. J. Zhu, Y. H. Liu, J. H. Yang and C. S. Wang, *Acs Nano*, 2013, **7**, 10995-11003.
6 J. B. Goodenough and Y. Kim, *Chem Mater*, 2010, **22**, 587-603.
7 J. X. Wu, X. Y. Qin, H. R. Zhang, Y. B. He, B. H. Li, L. Ke, W. Lv, H. D. Du, Q. H. Yang and F. Y. Kang, *Carbon*, 2015, **84**, 434-443.
8 Y. H. Xu, Y. J. Zhu, F. D. Han, C. Luo and C. S. Wang, *Adv Energy Mater*, 2015, **5**, 1400753.
9 K. Evanoff, A. Magasinski, J. B. Yang and G. Yushin, *Adv Energy Mater*, 2011, **1**, 495-498.
10 C. Martin, M. Alias, F. Christien, O. Crosnier, D. Belanger and T. Brousse, *Adv Mater*, 2009, **21**, 4735-4741.
11 X. Q. Yuan, H. X. Xin, X. Y. Qin, X. J. Li, Y. F. Liu and H. F. Guo, *Electrochim Acta*, 2015, **155**, 251-256.
12 X. S. Zhou, L. J. Wan and Y. G. Guo, *Small*, 2013, **9**, 2684-2688.
13 W. H. Lee, D. Y. Kang, J. S. Kim, J. K. Lee and J. H. Moon, *Rsc Adv*, 2015, **5**, 17424-17428.
14 W. Weng, H. J. Lin, X. L. Chen, J. Ren, Z. T. Zhang, L. B. Qiu, G. Z. Guan and H. S. Peng, *J Mater Chem A*, 2014, **2**, 9306-9312.
15 R. Epur, M. Ramanathan, M. K. Datta, D. H. Hong, P. H. Jampani, B. Gattu and P. N. Kumta, *Nanoscale*, 2015, **7**, 3504-3510.
16 Z. D. Lu, N. Liu, H. W. Lee, J. Zhao, W. Y. Li, Y. Z. Li and Y. Cui, *Acs Nano*, 2015, **9**, 2540-2547.
17 K. Fu, O. Yildiz, H. Bhanushali, Y. X. Wang, K. Stano, L. G. Xue, X. W. Zhang and P. D. Bradford, *Adv Mater*, 2013, **25**, 5109-5114.
18 L. Y. Beaulieu, K. W. Eberman, R. L. Turner, L. J. Krause and J. R. Dahn, *Electrochem Solid St*, 2001, **4**, A137-A140.
19 H. Tang, Y. J. Zhang, Q. Q. Xiong, J. D. Cheng, Q. Zhang, X. L. Wang, C. D. Gu and J. P. Tu, *Electrochimica Acta*, 2015, **156**, 86-93.
20 J.-H. Cho and S. T. Picraux, *Nano Lett*, 2014, **14**, 3088-3095.
21 Y. F. Chen, N. Du, H. Zhang and D. R. Yang, *J Alloy Compd*, 2015, **622**, 966-972.
22 Y. Wen, Y. J. Zhu, A. Langrock, A. Manivannan, S. H. Ehrman and C. S. Wang, *Small*, 2013, **9**, 2810-2816.
23 B. R. Liu, P. Soares, C. Checkles, Y. Zhao and G. H. Yu, *Nano Lett*, 2013, **13**, 3414-3419.
24 C. L. Ma, C. Ma, J. Z. Wang, H. Q. Wang, J. L. Shi, Y. Song, Q. G. Guo and L. Liu, *Carbon*, 2014, **72**, 38-46.
25 L. F. Cui, R. Ruffo, C. K. Chan, H. L. Peng and Y. Cui, *Nano Lett*, 2009, **9**, 491-495.
26 Z. S. Wen, Z. Y. Zhang and G. Q. Wang, *Rsc Adv*, 2014, **4**, 57430-57435.
27 H. Wu, G. Chan, J. W. Choi, I. Ryu, Y. Yao, M. T. McDowell, S. W. Lee, A. Jackson, Y. Yang, L. B. Hu and Y. Cui, *Nat Nanotechnol*, 2012, **7**, 309-314.
28 H. Ma, F. Y. Cheng, J. Chen, J. Z. Zhao, C. S. Li, Z. L. Tao and J. Liang, *Adv Mater*, 2007, **19**, 4067-4070.
29 U. Kasavajjula, C. S. Wang and A. J. Appleby, *J Power Sources*, 2007, **163**, 1003-1039.
30 X. J. Feng, J. Yang, Y. T. Bie, J. L. Wang, Y. N. Nuli and W. Lu, *Nanoscale*, 2014, **6**, 12532-12539.
31 W. Wang and P. N. Kumta, *Acs Nano*, 2010, **4**, 2233-2241.
32 S. L. Jing, H. Jiang, Y. J. Hu and C. Z. Li, *J Mater Chem A*, 2014, **2**, 16360-16364.
33 C. Wang, J. Ju, Y. Q. Yang, Y. F. Tang, H. Bi, F. H. Liao, J. H. Lin, Z. J. Shi, F. Q. Huang and R. P. S. Han, *Rsc Adv*, 2013, **3**, 21588-21595.
34 M. S. Wang, W. L. Song, J. Wang and L. Z. Fan, *Carbon*, 2015, **82**, 337-345.
35 H,Tang, J. Zhang, Q. Q. Xiong, Y. Li, X. L. Wang, C. D. Gu, and J. P. Tu, *J Power Sources*, 2015, **286**, 431-437
36 J. B. Chang, X. K. Huang, G. H. Zhou, S. M. Cui, P. B. Hallac, J. W. Jiang, P. T. Hurley and J. H. Chen, *Adv Mater*, 2014, **26**, 758-764.
37 J. Y. Ji, H. X. Ji, L. L. Zhang, X. Zhao, X. Bai, X. B. Fan, F. B. Zhang and R. S. Ruoff, *Adv Mater*, 2013, **25**, 4673-4677.
38 K. Evanoff, J. Benson, M. Schauer, I. Kovalenko, D. Lashmore, W. J. Ready and G. Yushin, *Acs Nano*, 2012, **6**, 9837-9845.
39 M. N. Hyder, B. M. Gallant, N. J. Shah, Y. Shao-Horn and P. T. Hammond, *Nano Lett*, 2013, **13**, 4610-4619.
40 Z. Shi, X. J. Chen, X. W. Wang, T. Zhang and J. Jin, *Adv Funct Mater*, 2011, **21**, 4358-4363.
41 S. W. Lee, B. S. Kim, S. Chen, Y. Shao-Horn and P. T. Hammond, *J Am Chem Soc*, 2009, **131**, 671-679.
42 X. S. Zhou, Y. X. Yin, L. J. Wan and Y. G. Guo, *Adv Energy Mater*, 2012, **2**, 1086-1090.
43 W. Y. Li, Y. B. Tang, W. P. Kang, Z. Y. Zhang, X. Yang, Y. Zhu, W. J. Zhang and C. S. Lee, *Small*, 2015, **11**, 1345-1351.
44 J. G. Ren, C. D. Wang, Q. H. Wu, X. Liu, Y. Yang, L. F. He and W. J. Zhang, *Nanoscale*, 2014, **6**, 3353-3360.

